Award Number: W81XWH-10-1-0357

TITLE: Studying the Role of Eukaryotic Translation Initiation Factor 4E (eIF4E) Phosphorylation by MNK1/2 Kinases in Prostate Cancer Development and Progression

PRINCIPAL INVESTIGATOR: Bruno Fonseca

CONTRACTING ORGANIZATION: Royal Institution for the Advancement of Learning

Montreal H3A 2T5

REPORT DATE: June 2012

TYPE OF REPORT: Annual Summary

PREPARED FOR: U.S. Army Medical Research and Materiel Command
                        Fort Detrick, Maryland 21702-5012

DISTRIBUTION STATEMENT: Approved for Public Release;
                        Distribution Unlimited

The views, opinions and/or findings contained in this report are those of the author(s) and should not be construed as an official Department of the Army position, policy or decision unless so designated by other documentation.

REPORT DOCUMENTATION PAGE

Form Approved
OMB No. 0704-0188

Public reporting burden for this collection of information is estimated to average 1 hour per response, including the time for reviewing instructions, searching existing data sources, gathering and maintaining the data needed, and completing and reviewing this collection of information. Send comments regarding this burden estimate or any other aspect of this collection of information, including suggestions for reducing this burden to Department of Defense, Washington Headquarters Services, Directorate for Information Operations and Reports (0704-0188), 1215 Jefferson Davis Highway, Suite 1204, Arlington, VA 22202-4302. Respondents should be aware that notwithstanding any other provision of law, no person shall be subject to any penalty for failing to comply with a collection of information if it does not display a currently valid OMB control number. **PLEASE DO NOT RETURN YOUR FORM TO THE ABOVE ADDRESS.**

1. REPORT DATE	2. REPORT TYPE	3. DATES COVERED
June 2012	Annual Summary	1 JUN 2011 - 31 MAY 2012

4. TITLE AND SUBTITLE

Studying the Role of Eukaryotic Translation Initiation Factor 4E (eIF4E) Phosphorylation by Mnk1/2 Kinases in Prostate Cancer Development and Progression

5a. CONTRACT NUMBER

5b. GRANT NUMBER
W81XWH-10-1-0357

5c. PROGRAM ELEMENT NUMBER

6. AUTHOR(S)

Bruno Fonseca

E-Mail: bd.fonseca@mcgill.ca

5d. PROJECT NUMBER

5e. TASK NUMBER

5f. WORK UNIT NUMBER

7. PERFORMING ORGANIZATION NAME(S) AND ADDRESS(ES)

Royal Institution for the Advancement of Learning
Montreal (H3A 1A3), Quebec, Canada

8. PERFORMING ORGANIZATION REPORT NUMBER

9. SPONSORING / MONITORING AGENCY NAME(S) AND ADDRESS(ES)
U.S. Army Medical Research and Materiel Command
Fort Detrick, Maryland 21702-5012

10. SPONSOR/MONITOR'S ACRONYM(S)

11. SPONSOR/MONITOR'S REPORT NUMBER(S)

12. DISTRIBUTION / AVAILABILITY STATEMENT
Approved for Public Release; Distribution Unlimited

13. SUPPLEMENTARY NOTES

14. ABSTRACT

The mRNA cap-binding protein eukaryotic initiation factor 4E (eIF4E) plays a key role in cancer progression. We have recently shown (Furic *et al.*, 2010) that phosphorylation of eIF4E at Ser209 by the MNK family of kinases promotes prostate cancer progression in a mouse model bearing a tissue-specific conditional PTEN deletion in prostatic epithelia. eIF4E activity is regulated at two levels: phosphorylation of Ser209 and binding to a family of small eIF4E-binding proteins aptly termed 4E-BPs. Binding of 4E-BPs to eIF4E precludes eIF4G binding thus preventing assembly of the eIF4F complex and recruitment of the ribosome to the messenger RNA. Our most recent data suggests that PTEN interacts genetically with 4E-BPs to induce cellular senescence in prostate cancer. In this report, we also begin to address the effects of simultaneous inhibition of MNK and mTORC1 activity in anchorage-independent prostate cancer cell lines. Our findings will hopefully yield important information for the design of effective therapeutic agents against human prostate cancer.

15. SUBJECT TERMS
 eIF4E phosphorylation, MNKs, mTORC1, 4E-BPs, cellular senescence, anchorage-independent growth

16. SECURITY CLASSIFICATION OF:			17. LIMITATION OF ABSTRACT	18. NUMBER OF	19a. NAME OF RESPONSIBLE PERSON USAMRMC
a. REPORT	**b. ABSTRACT**	**c. THIS PAGE**	UU	27	19b. TELEPHONE NUMBER *(include area code)*
U	U	U			

Annual Progress Report

Table of Contents   *Page number*

1. Introduction

The mRNA cap-binding protein eukaryotic initiation factor 4E (eIF4E) is a key player in cancer development (Mamane *et al.*, 2004). Overexpression of eIF4E in NIH 3T3 and Rat-2 fibroblasts causes their oncogenic transformation (Lazaris-Karatzas *et al.*, 1990). Specifically, overexpression of eIF4E induces foci formation on a cell monolayer and allows for anchorage-independent growth. Moreover, injection of cell lines overexpressing eIF4E into nude mice leads invariably to tumor formation. eIF4E is phosphorylated on a single residue (Ser^{209}) (Furic *et al.*, 2010). Phosphorylation of this amino acid is believed to regulate eIF4E binding to the mRNA cap and the rate of protein synthesis. While it is still not clear whether phosphorylation of eIF4E enhances or decreases the rate of protein synthesis, a recent study from our lab by Furic *et al.* (2010) has shown that phosphorylation of eIF4E promotes prostate cancer development. This study used a mouse model of prostate cancer in which the tumor suppressor PTEN (a PIP$_3$ phosphatase) is deleted in the prostate epithelium (*Pten*$^{Flox/Flox}$; Probasin-Cre4).

2. Body

        Pten-null mice develop prostate invasive carcinoma by 5 to 8 months of age with complete penetrance (Trotman *et al.,* 2003). We observed that that $Pten^{Flox/Flox}/eIF4E^{Ser209A/Ser209A}$ mice had a lower incidence of high grade PIN (prostatic intraepithelial neoplasia) than $Pten^{Flox/Flox}/ eIF4E^{WT/WT}$ mice (Furic *et al.,* 2010), suggesting that eIF4E phosphorylation plays an important role in promoting prostate cancer tumorigenesis in the context of *Pten*-deficiency. In addition to being regulated by phosphorylation, the activity of eIF4E is also regulated indirectly by a family of small eIF4E-binding proteins termed 4E-BPs, which comprise 4E-BP1, 4E-BP2 and 4E-BP3. In their dephosphorylated state, 4E-BPs bind to eIF4E thereby displacing eIF4G and inhibiting eIF4F assembly which mediates recruitment of the ribosome to the mRNA. 4E-BPs play an important role in restraining tumor development. Mice lacking 4E-BP1, 4E-BP2 and p53 exhibit lower tumor-free survival than p53-null mice (Petrolakis *et al.,* 2009). Notably, the deletion of 4E-BP1 and 4E-BP2 alone caused cellular senescence *via* p53 (unrestrained cell growth depends upon simultaneous deletion of 4E-BP1, 4E-BP2 and p53 [Petrolakis *et al.*, 2009]). Cellular senescence is an irreversible form of cell cycle arrest that can be triggered by inactivation of tumor suppressors or activation of proto-oncogenes. It occurs in aged prostate epithelia and can be readily monitored by SA-β-galactosidase staining (Fig. 2A). Deletion of PTEN (like 4E-BP1/4E-BP2) leads to p53-dependent cellular senescence (Chen *et al.,* 2005). PTEN regulates 4E-BP phosphorylation levels via mTORC1 (Fig. 1). We sought to investigate whether acute PTEN loss caused cellular senescence *via* the 4E-BPs. To address this possibility, *4E-BP1/4E-BP2* double knockout mice were crossed with *Pten*-conditional knockout mice to generate *4E-BP1/4E-BP2* WT/*Pten*$^{Flox/Flox}$, *4E-BP1/4E-BP2* heterozygous/*Pten*$^{Flox/Flox}$ and *4E-BP1/4E-BP2 DKO/PTEN*$^{Flox/Flox}$ mice. The SA-β-galactosidase staining for 4E-BPs WT, heterozygous and null prostate epithelia was indistinguishable, *i.e.* no additive staining was observed upon deletion of 4E-BP1 and 4E-BP2 (Fig. 2B). These preliminary data suggest that loss of PTEN leads to senescence *via* the 4E-BPs. We have shown previously (Furic *et al.,* 2010) that eIF4E phosphorylation is required for anchorage-independent growth in *Pten*$^{Flox/Flox}$ mouse embryo fibroblasts (MEFs) transduced with SV40-large T antigen. Since 4E-BP phosphorylation is regulated by PTEN, next we assessed whether 4E-BP phosphorylation plays a role in anchorage-independent growth. Phosphorylation of 4E-BPs is catalyzed by the serine/threonine protein kinase complex mammalian target of rapamycin complex 1 (mTORC1). Inhibition of mTORC1 with the allosteric inhibitor, rapamycin or the kinase inhibitor PP242 almost abolished anchorage – independent growth (Fig. 3A). Inhibition of MNK activity with compound 3 (CPD3) resulted in a substantial decrease in the number of colonies formed in soft agar. Simultaneous incubation of mTORC1 with MNK inhibitors did not have an additive effect on anchorage-independent growth, presumably because the mTORC1 inhibition alone almost completely abrogates anchorage independent growth. Therefore, it is difficult to conclude whether MNKs and mTORC1 regulate anchorage independence throught the same molecular mechanism. As expected, rapamycin and PP242 (but not CPD3) markedly reduced the phosphorylation of ribosomal

protein S6, a maker for mTORC1 activation. Next we will confirm the inhibitory effect of CPD3 on MNK activity, using a phospho-specific antibody against eIF4E.

3. Key research accomplishments

- Demonstration that eIF4E phosphorylation is paramount for prostate cancer development in mouse models bearing a conditional PTEN deletion in prostatic epithelia (Furic *et al.,* 2010).

- Demonstration that cellular senescence in prostate cancer observed upon acute loss of PTEN loss likely results from increased phosphorylation of 4E-BPs (appendix, unpublished).

- Demonstration that inhibition MNK or mTORC1 signaling have similar outcomes with regards to inhibition of anchorage-independent growth (appendix, unpublished).

4. Reportable outcomes

Furic L, Rong L, Larsson O, Koumakpayi IH, Yoshida K, Brueschke A, Petroulakis E, Robichaud N, Pollak M, Gaboury LA, Pandolfi PP, Saad F, Sonenberg N. *eIF4E phosphorylation promotes tumorigenesis and is associated with prostate cancer progression.* Proc Natl Acad Sci U S A. 2010 Aug 10;107(32):14134-9.

5. Conclusion

In future work, we will repeat the preliminary data (shown in Fig. 3) to confirm our findings. We will also evaluate the effect of simultaneous MNK and mTORC1 inhibition on cell proliferation of human prostate cancer PC-3 cells. To this end,we will use a well-established BrdU labeling assay to quantify cells actively cycling through S-phase. We will validate our BrdU cell assay findings by trypan-blue exclusion viable cell counting. Should we observe an additive or synergistic effect of MNK and mTORC1 inhibition on cell proliferation, we will test the effect of simultaneous inhibition of these two pathways on tumor growth *in vivo*. Specificlly we will inject PC-3 cells in nude mice subcutaneously, allow tumors to develop to a palpable size and subsequently inject rapamycin, PP242 and/or CPD3 into the tail vein. Tumors will be excised and size measured. Samples of tumors will be analysed for mTORC1 and MNK activation with phosphor-specific antisera against phosphorylated ribosomal protein S6 and eIF4E.

6. References

Chen Z, Trotman LC, Shaffer D, Lin HK, Dotan ZA, Niki M, Koutcher JA, Scher HI, Ludwig T, Gerald W, Cordon-Cardo C, Pandolfi PP. *Crucial role of p53-dependent cellular senescence in suppression of Pten-deficient tumorigenesis.* Nature. 2005 Aug 4;436(7051):725-30.

Furic L, Rong L, Larsson O, Koumakpayi IH, Yoshida K, Brueschke A, Petroulakis E, Robichaud N, Pollak M, Gaboury LA, Pandolfi PP, Saad F, Sonenberg N. *eIF4E phosphorylation promotes tumorigenesis and is associated with prostate cancer progression.* Proc Natl Acad Sci U S A. 2010 Aug 10;107(32):14134-9.

Lazaris-Karatzas A, Montine KS, Sonenberg N. *Malignant transformation by a eukaryotic initiation factor subunit that binds to mRNA 5' cap.* Nature. 1990 Jun 7;345(6275):544-7.

Mamane Y, Petroulakis E, Rong L, Yoshida K, Ler LW, Sonenberg N. *eIF4E-from translation to transformation.* Oncogene. 2004 Apr 19;23(18):3172-9.

Petroulakis E, Parsyan A, Dowling RJ, LeBacquer O, Martineau Y, Bidinosti M, Larsson O, Alain T, Rong L, Mamane Y, Paquet M, Furic L, Topisirovic I, Shahbazian D, Livingstone M, Costa-Mattioli M, Teodoro JG, Sonenberg N. *p53-dependent translational control of senescence and transformation via 4E-BPs.* Cancer Cell. 2009 Nov 6;16(5):439-46.

Trotman LC, Niki M, Dotan ZA, Koutcher JA, Di Cristofano A, Xiao A, Khoo AS, Roy-Burman P, Greenberg NM, Van Dyke T, Cordon-Cardo C, Pandolfi PP. *Pten dose dictates cancer progression in the prostate.* PLoS Biol. 2003 Dec;1(3):E59.

7. Appendix

eIF4E phosphorylation promotes tumorigenesis and is associated with prostate cancer progression

Luc Furic[a,1], Liwei Rong[a], Ola Larsson[a], Ismaël Hervé Koumakpayi[b], Kaori Yoshida[a], Andrea Brueschke[a], Emmanuel Petroulakis[a], Nathaniel Robichaud[a], Michael Pollak[c], Louis A. Gaboury[d], Pier Paolo Pandolfi[e], Fred Saad[b], and Nahum Sonenberg[a]

[a]Goodman Cancer Centre and Department of Biochemistry, Cancer Pavilion, McGill University, Montreal, QC, Canada H3A 1A3; [b]Department of Surgery, Hôpital Notre-Dame, Centre Hospitalier de l'Université de Montréal, Université de Montréal, Montreal, QC, Canada H2L 4M1; [c]Departments of Medicine and Oncology and Segal Cancer Center, McGill University, Montreal, QC, Canada H3T 1E2; [d]Institut de Recherche en Immunologie et Cancérologie, Université de Montréal, Montréal, Montreal, QC, Canada H3T 1J4; and [e]Beth Israel Deaconess Cancer Center and Departments of Medicine and Pathology, Beth Israel Deaconess Medical Center, Harvard Medical School, Boston, MA 02115

Translational regulation plays a critical role in the control of cell growth and proliferation. A key player in translational control is eIF4E, the mRNA 5′ cap-binding protein. Aberrant expression of eIF4E promotes tumorigenesis and has been implicated in cancer development and progression. The activity of eIF4E is dysregulated in cancer. Regulation of eIF4E is partly achieved through phosphorylation. However, the physiological significance of eIF4E phosphorylation in mammals is not clear. Here, we show that knock-in mice expressing a nonphosphorylatable form of eIF4E are resistant to tumorigenesis in a prostate cancer model. By using a genome-wide analysis of translated mRNAs, we show that the phosphorylation of eIF4E is required for translational up-regulation of several proteins implicated in tumorigenesis. Accordingly, increased phospho-eIF4E levels correlate with disease progression in patients with prostate cancer. Our findings establish eIF4E phosphorylation as a critical event in tumorigenesis. These findings raise the possibility that chemical compounds that prevent the phosphorylation of eIF4E could act as anticancer drugs.

PTEN | translational control

Aberrations in the control of mRNA translation initiation have been documented in many tumor types (1–4). Translation initiation is controlled in part by eIF4E, the mRNA 5′ cap-binding protein. eIF4E is a proto-oncogene, inasmuch as its overexpression in immortalized rodent fibroblasts or human epithelial cells causes transformation (5, 6), and in mouse models its overexpression engenders tumor formation (7, 8). eIF4E is phosphorylated by the MNK1/2 serine/threonine kinases, which are activated in response to mitogenic and stress signaling downstream of ERK1/2 and p38 MAP kinase, respectively (9, 10). eIF4E phosphorylation at serine 209 by MNK1/2 promotes its transformation activity (11, 12). To study the role of eIF4E phosphorylation in tumorigenesis in the whole organism, we generated a knock-in (KI) mouse in which eIF4E serine 209 was mutated to alanine. Here, we show that mouse embryonic fibroblasts (MEFs) isolated from eIF4E$^{S209A/S209A}$ embryos display a marked resistance to oncogene-induced transformation. Furthermore, the mutant mice are viable, but are resistant to development of *Pten* loss–induced prostate cancer, and this resistance is associated with a decrease in MMP3, CCL2, VEGFC, and BIRC2 proteins. Moreover, eIF4E is highly phosphorylated in hormone-refractory prostate cancer, which correlates with poor clinical outcome. These results demonstrate the importance of eIF4E phosphorylation in tumorigenesis and validate the eIF4E phosphorylation pathway as a potential therapeutic target for cancer.

Results

Ser209 Is the Only Phosphorylation Site in eIF4E.
To address the role of eIF4E phosphorylation in tumorigenesis, a knock-in (KI) mouse in which serine 209 was replaced by an alanine residue was generated. The strategy and targeting vector construction for the generation, selection, and genotyping of the S209A mice is shown in Fig. S1. The eIF4E$^{S209A/S209A}$ mice (referred to as KI mice hereafter) showed no obvious phenotype. To determine whether S209 is the only phosphorylation site on eIF4E, orthophosphate labeling of MEFs isolated from WT and KI littermate embryos was performed. Phosphorous 32–radiolabeled eIF4E was detected by immunoprecipitation in only WT MEFs (Fig. 1A). As expected, TPA stimulation, which activates MNK (13), induced a twofold increase in eIF4E phosphorylation (Fig. 1A). Thus, mutating S209 abrogates eIF4E phosphorylation.

eIF4E-KI MEFs Are Resistant to RAS-Induced Transformation.
RAS is an upstream activator of MNK1 and MNK2 through ERK-1 and -2 (9, 10). Therefore, it was pertinent to determine whether transformation by RAS is facilitated by eIF4E phosphorylation. To this end, the two-oncogene transformation assay was performed with retroviruses expressing RAS^{V12} (RAS containing the activating mutation G12V) together with c-MYC or E1A. Experiments were carried out in primary MEFs between passages three and five. Strikingly, KI MEFs infected with a combination of retroviruses expressing RAS^{V12} and c-MYC formed approximately fivefold fewer foci than WT MEFs (Fig. 1B). A similar difference in transformation efficiency was observed when MEFs were infected with retroviruses expressing the adenovirus E1A together with RAS^{V12} (Fig. 1B). WT and KI MEFs infected with an empty retrovirus failed to form foci (Fig. 1B). Anchorage-independent growth of WT and KI MEFs transduced with activated RAS^{V12} and c-MYC was determined by colony formation in soft agar. The assay was performed with three different pairs of MEFs, each isolated from embryos of a different pregnant mouse. KI MEFs formed four- to 10-fold fewer colonies than WT MEFs (Fig. 1C). These results demonstrate that eIF4E phosphorylation on serine 209 is required for efficient transformation by RAS. To further demonstrate the importance of eIF4E phosphorylation for cellular transformation, we performed transformation assays using immortalized WT or MNK1/2 DKO MEFs and HA-tagged eIF4E as the transforming oncogene. HA-tagged eIF4E was expressed at similar levels in WT and MNK1/2 DKO MEFs, and as expected no phosphorylation of endogenous or HA-tagged eIF4E was detected by Western blotting in MNK1/2 DKO MEFs (Fig. 1D). WT MEFs overexpressing HA-eIF4E formed foci after

Fig. 1. KI MEFs are resistant to malignant transformation. (A) Untreated or TPA-treated (100 ng/mL) MEFs were labeled with ^{32}P-orthophosphate for 2 h as described in *Materials and Methods*. Cells were lysed and the supernatant was incubated with control (preimmune serum) or eIF4E antibody. Immunoprecipitated proteins were resolved by SDS/PAGE followed by autoradiography and Western blotting. (B) MEFs infected with the indicated retroviruses were grown on a monolayer and focus formation was determined after 10 d in culture by methylene blue staining. Similar results were obtained with eight independent pairs of MEFs. (C) WT and KI MEFs infected with c-MYC and RAS^{V12} expression vectors were grown in soft agar and the total number of colonies consisting of more than eight cells were counted (six wells for each pair of MEFs). WT MEFs formed significantly more colonies than KI MEFs (two-tailed Student t test, P = 0.037). (D) Cell lysates from WT and MNK1/2 DKO MEFs expressing HA-eIF4E were resolved by SDS/PAGE followed by Western blotting. Arrows indicate the slower migrating band corresponding to the HA-tagged eIF4E. (E) MEFs infected with the indicated retroviruses were grown on a monolayer and focus formation was determined after 10 d in culture by methylene blue staining. (F and G) Cells (1 × 10^5) were seeded on d 0 and counted on d 1, 3, and 5. Data points represent mean ± SD of three independent experiments. (H) Cells (1 × 10^6) were seeded and subjected to treatment for 24 h with the indicated concentrations of ionomycin. Floating and attached

cells were collected, and the double-positive Annexin V/PI subpopulation of cells was gated. No significant differences were observed between WT and KI MEFs (two-tailed Student t test: not treated, P = 0.511; 10 μM, P = 0.329; 15 μM, P = 0.952). Similar results were obtained in three independent experiments. (I) MEFs were serum starved for 6 h in the presence of vehicle (DMSO), PP242 (2.5 μM), or Torin1 (250 nM), serum-stimulated for 30 min, and the phosphorylation and levels of indicated proteins were determined by Western blotting. (J) Raptor was silenced in HEK293 cells by shRNA (sh-raptor). As a control, cells were infected with a lentivirus encoding a scrambled shRNA. Expression and the phosphorylation levels of the indicated proteins were determined by Western blotting. (K) WT/PTEN$^{F/F}$ and KI/PTEN$^{F/F}$ MEFs infected with the indicated retroviruses were grown as a monolayer and focus formation was determined after 10 d in culture by methylene blue staining. Similar results were obtained from two independent experiments each done in triplicate.
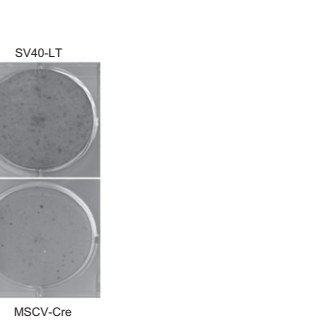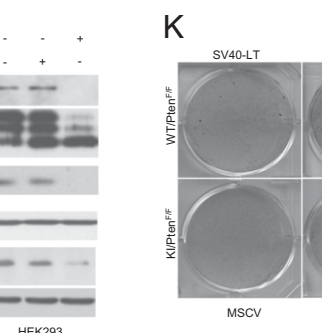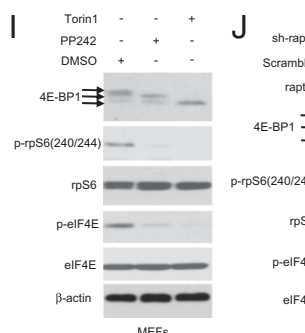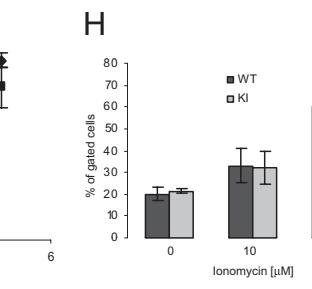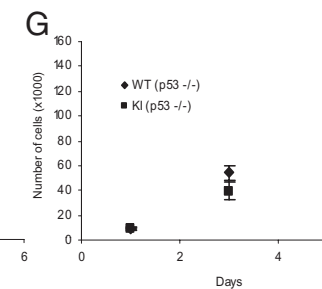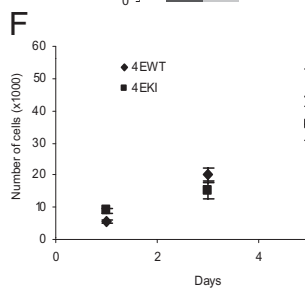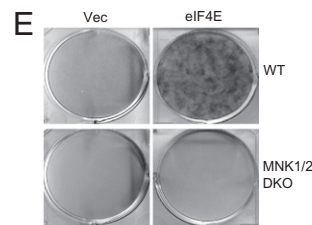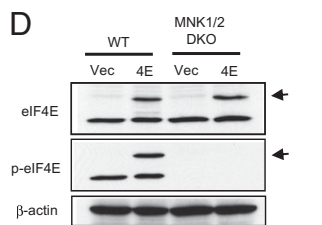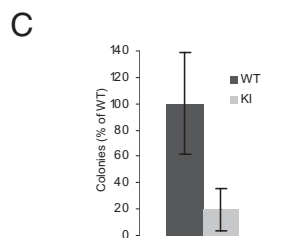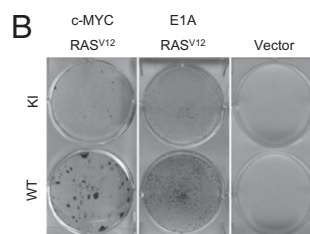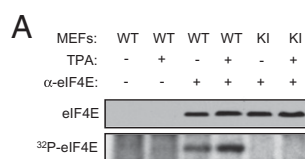
10 d in culture. Strikingly, MNK1/2 DKO MEFs were completely resistant to transformation by HA-eIF4E (Fig. 1*E*). These findings clearly demonstrate that eIF4E transforming activity is absolutely dependent on phosphorylation by the MNK1/2 kinases.

Abrogating eIF4E Phosphorylation Does Not Impair Cell Proliferation. The resistance of KI MEFs to transformation could be explained by an inherently reduced proliferative rate of KI MEFs compared with WT MEFs. To investigate this possibility, growth curves using primary MEFs at passage three were performed. No difference in growth between WT and KI MEFs over a 5-d period was detected (Fig. 1*F*). Primary MEFs are slow-growing cells and consequently a small effect on growth could have been missed. We therefore crossed the WT and the KI mice with p53-null mice to generate immortalized WT and KI MEFs, which grow faster than primary MEFs. Similar growth curves were obtained for both WT and KI p53-null MEFs (Fig. 1*G*). Another

possible explanation for the reduced transformation efficiency of KI MEFs is that they are more susceptible to apoptosis. To address this possibility, WT and KI primary MEFs were treated with the apoptosis inducing ionophore ionomycin. Apoptotic and necrotic cells were visualized by dual annexin V–propidium iodide staining. No difference in the percentage of apoptotic and necrotic cells was observed between WT and KI MEFs after ionomycin treatment (Fig. 1*H*). In addition, there was no difference in cell cycle progression or apoptosis between WT and KI cells transformed by c-MYC and RAS^{V12} (Fig. S2 *A*–*C*). These results indicate that the resistance of KI MEFs to Ras-induced transformation cannot be explained by decreased proliferation or increased cell death.

eIF4E Phosphorylation Is Regulated by Mammalian Target of Rapamycin Complex 1 and Contributes to Transformation via the PI3K Pathway. Another pathway that controls eIF4E activity is the PI3K pathway

via the phosphorylation of the suppressor 4E-BPs by mammalian target of rapamycin complex 1 (mTORC1) (1, 14). The loss of the tumor suppressor PTEN leads to AKT, and subsequent mTORC1 activation (15). To determine whether eIF4E phosphorylation is impacted by mTORC1, we treated immortalized MEFs with two active-site inhibitors of mTORC1, Torin1 (16) and PP242 (17). Inhibition of the mTORC1 kinase was confirmed by a decrease in the phosphorylation of the small ribosomal subunit protein S6 (p-rpS6) and 4E-BP1 (Fig. 1*I*). Interestingly, eIF4E phosphorylation was drastically diminished following mTORC1 inhibition (Fig. 1*I*). To confirm that the decrease in eIF4E phosphorylation was not a result of nonspecific effects of the two inhibitors, we used shRNA-mediated knockdown of RAPTOR as an alternative approach for inhibiting mTORC1 activity in 293 cells. Consistent with the results obtained with Torin1 and PP242, lowering the amount of RAPTOR caused a marked decrease in eIF4E phosphorylation (Fig. 1*J*). These results can be readily explained by the fact that dephos-

phorylation of 4E-BPs increases their binding to eIF4E, thus preventing eIF4E binding to eIF4G, on which MNK docks (18). We investigated further the role of eIF4E phosphorylation control downstream of mTORC1 by generating WT and KI MEFs in which both alleles of PTEN were deleted via CRE-mediated recombination (15). MEFs were immortalized with SV40 largeT and subsequently infected with a CRE-expressing retrovirus to delete *Pten*. Loss of PTEN in combination with SV40 large T expression caused malignant transformation as determined by focus formation in WT MEFs, whereas KI MEFs were resistant to transformation, as only a few foci were detected (Fig. 1*K*). These results demonstrate that eIF4E phosphorylation is involved in PTEN loss–driven cellular transformation.

eIF4E-KI Mice Are Resistant to PTEN Loss-Induced Prostate Cancer. Because *Pten* deletion is expected to result in increased eIF4E phosphorylation, we investigated the importance of eIF4E phos-

Fig. 2. KI mice are resistant to Pten loss–induced prostate cancer. (*A–I*) Representative H&E staining of sections from the anterior (AP), ventral (VP), and DLP lobes of the prostate of WT, WT/cPten^F/F, and KI/cPten^F/F from 5- to 6-mo-old mice (no histological difference was observed between WT and KI mice without Cre; Fig. S3). (Scale bar: 100 μm.) (*J*) Histograms represent percentage of predominant lesions in a cohort of seven WT/cPten^F/F and seven KI/cPten^F/F. (*K* and *L*) Representative images of Ki67 staining of DLP sections from WT/cPten^F/F and KI/cPten^F/F mice (5–6 mo old). (Scale bar: 100 μm.) (*M*) Slides were scanned with the Aperio Scanscope and nuclear staining was quantified with the Image Scope software nuclear algorithm. At least 4,000 nuclei per mouse were analyzed (*n* = 4 mice per group). Student *t* test (two-tailed) was performed. (*N–S*) Ventral prostate sections from WT, WT/cPten^F/F, and KI/cPten^F/F mice were used for IHC with the indicated antibodies. (Scale bar: 50 μm.)

phorylation in tumor formation in vivo in a mouse model of prostate cancer in which the tumor suppressor *Pten* is deleted in the prostate epithelium (*Pten*$^{Flox/Flox}$; PB-Cre4) (15). These mice develop invasive carcinoma by 5 to 8 mo of age with complete penetrance (15). KI mice were crossed with *Pten*-conditional KO mice to generate *eIF4E* WT/*Pten*$^{Flox/Flox}$/PB-Cre4 and *eIF4E* KI/*Pten*$^{Flox/Flox}$/PB-Cre4, hereafter referred to as WT/cPten$^{F/F}$ and KI/cPten$^{F/F}$, respectively. Seven mice of each genotype were killed between the ages of 5 and 7 mo (Table S1). Cancerous lesions, mainly prostatic intraepithelial neoplasia (PIN), were graded from I to IV (Fig. S4 shows representative sections) (19, 20). Analysis of H&E-stained sections of all prostate lobes in 5- to 7-mo-old mice shows that KI/cPten$^{F/F}$ mice had a lower incidence of high grade PIN (represented by PIN IV lesions) than WT/cPten$^{F/F}$ mice (Fig. 2 *A–I*). There was a significant difference in the grade of lesions observed between WT/cPten$^{F/F}$ and KI/cPten$^{F/F}$ mice (*P* = 0.038, Mann–Whitney *U* test). The distribution of the lesions in WT/cPten$^{F/F}$ and KI/cPten$^{F/F}$ is shown in Fig. 2*J*. It is noteworthy that no infiltrating adenocarcinoma was observed in KI/cPten$^{F/F}$. It is unlikely that the differences seen in the severity of the lesions between WT/cPten$^{F/F}$ and KI/cPten$^{F/F}$ are caused by a small delay in tumor appearance, as the median age at sacrifice time was 25 wk for the KI/cPten$^{F/F}$ compared with 20 wk for the WT/cPten$^{F/F}$ mice (Table S1). The differences in the severity of the lesions between the WT and KI groups were also determined by the number of proliferative cells as detected by Ki67 staining in the dorsolateral prostate (DLP) of mice from each genotype (Fig. 2 *K–L*). DLP was chosen because it is histologically and functionally the most closely related to the peripheral zone of the human prostate (21), which is the region where most prostate cancers occur in men (22, 23). There was a significant decrease (*P* = 0.013) in the number of Ki67-positive nuclei between WT/cPten$^{F/F}$ (24.5 ± 6.6%) and KI/cPten$^{F/F}$ (9.5 ± 1.1%) mice (Fig. 2*M*). In addition, eIF4E was highly phosphorylated on Ser209 in PIN IV lesions from WT/cPten$^{F/F}$ mice (Fig. 2 *N–P*). AKT^{Ser473} phosphorylation was increased to the same extent in WT/cPten$^{F/F}$ and KI/cPten$^{F/F}$ mice (Fig. 2 *Q–S*), suggesting that differences in lesion grade are not caused by a weaker activation of the PI3K pathway in the KI mice. Taken together, these results demonstrate that eIF4E phosphorylation plays an important role in *Pten* loss–induced tumorigenesis.

eIF4E Phosphorylation Increases the Translation Efficiency of a Subset of mRNAs Encoding Protumorigenic Factors. To study the molecular basis that underlies the eIF4E-KI resistance to tumorigenesis at the translational level, polysome profiling was performed on WT and KI immortalized MEFs. The changes in distribution of mRNAs along a sucrose density gradient between WT and KI MEFs were studied using DNA oligonucleotide microarrays. mRNAs in KI MEFs that shifted to lighter fractions relative to WT MEFs in the density gradient, after correcting for total cytoplasmic mRNA levels, are expected to be translated less efficiently in KI MEFs. A list of 35 mRNAs that exhibited the most pronounced shifts is shown in Table S2. Among these mRNAs are the chemokines *Ccl2* and *Ccl7* that are implicated in tumor progression. Targeting CCL2 with a neutralizing antibody caused prostate tumor regression (24–26). The list also includes mRNAs encoding the matrix metalloproteinases (MMPs) MMP3 and MMP9, which are overexpressed in PC3 prostate cancer cells (27), and promote invasion and metastasis by rearrangement of the ECM (28, 29). Other mRNAs encode the inhibitor of apoptosis, baculoviral IAP repeat–containing protein 2 (BIRC2), and the growth factor VEGFC. To determine whether the differences in polysome sedimentation between WT and KI MEFs are reflected in changes in the abundance of protein, we examined VEGFC, BIRC2, MMP3, and nuclear factor of κ-light polypeptide gene enhancer in B-cells inhibitor-α (NFKBIA; also known as IκBα) proteins by Western blotting (Fig. 3*A*). A 1.7- to 4.8-fold reduction in the amount of these proteins was observed in KI MEFs compared with WT MEFs, whereas the amount of AKT, eIF4E, and β-actin remained unchanged. In addition,

inhibiting Mnk1/2 kinases in two prostate cancer cell lines with the inhibitor CGP57380 (30) led to a decrease in the amount of VEGFC, BIRC2, and NFKBIA proteins (Fig. S5*A*). We also examined the amount of MMP3 in DLP extracts isolated from KI/cPten$^{F/F}$ and WT/cPten$^{F/F}$ mice. A fourfold decrease in MMP3 protein in the DLP of KI/cPten$^{F/F}$ compared with WT/cPten$^{F/F}$ was detected, whereas the protein was barely detected in DLP from WT mice (Fig. 3*B*). Considering that the KI mice develop fewer PIN IV lesions, characterized by a loss of the fibromuscular layer around the prostatic ducts (20), as seen by staining for smooth muscle actin (SMA; Fig. 3 *C–E*), MMP3 staining by immunohistochemistry (IHC) was performed. Consistent with the Western blotting data, MMP3 staining intensity was weaker in the prostate of KI/cPten$^{F/F}$ compared with WT/cPten$^{F/F}$ mice (Fig. 3 *F–H*). In addition, CCL2 staining in the prostate of KI/cPten$^{F/F}$ was weaker compared with WT/cPten$^{F/F}$ mice (Fig. 3 *I–K*). These results demonstrate that several mRNAs important for tumor progression are differentially translated in WT versus KI MEFs. Impairment in the remodeling of the extracellular matrix or differences in paracrine signaling could be possible explanations for the resistance of KI mice to Pten loss–induced tumorigenesis.

eIF4E Phosphorylation Is Associated with High Gleason Score and Strongly Correlates with MMP3 Expression in a Cohort of Patients with Prostate Cancer. Next, we investigated the correlation between eIF4E phosphorylation in human prostate cancer and disease progression. A tissue microarray (TMA) constructed with human prostate cancer (PCa) samples including patients presenting primary and hormone-refractory PCa (HR PCa) was used (31, 32). Both eIF4E and phospho-eIF4E staining intensity in-
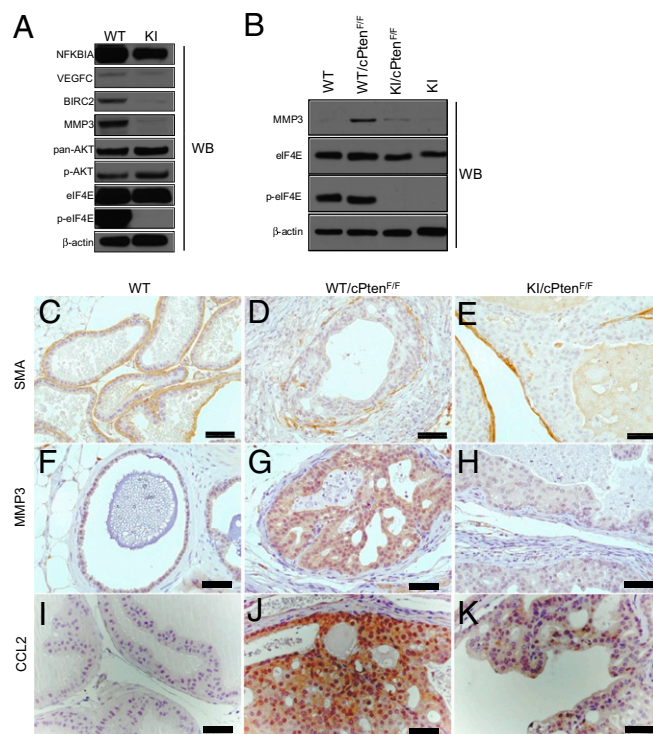
Fig. 3. Differential expression of selected proteins in prostate from WT versus KI mice. (*A*) Serum starved WT and KI MEFs were serum-stimulated for 2 h and cell lysates were resolved by SDS/PAGE followed by Western blotting with the indicated antibodies. (*B*) DLP extracts were resolved by SDS/PAGE and Western blotting with the indicated antibodies was performed. (*C–K*) Sections of the prostate from WT, WT/cPten$^{F/F}$, and KI/cPten$^{F/F}$ mice were used for IHC with the indicated antibodies. VP sections were used for detection of SMA and MMP3. CCL2 was detected in the anterior prostate. (Scale bar: 50 μm.)

creased gradually from normal to PIN, to hormone-sensitive (HS), and further to HR PCa tumors (Fig. 4*A* shows representative staining). Increased phospho-eIF4E and total eIF4E staining was significantly associated with HR tumors (Fig. 4 *B* and *C*). Statistical analysis of the association between phospho-eIF4E staining and Gleason grading demonstrated that tumors presenting with a Gleason score greater than 7 displayed a statistically significant increase in staining compared with tumors with a Gleason score of 7 or lower (Fig. 4*D*). Thus, there is a strong association between the degree of eIF4E phosphorylation and progression of prostate cancer to its deadliest stage. To determine whether MMP3 could also serve as a marker of prostate cancer progression, we stained the same TMA for the presence of MMP3 (Fig. 4*A* shows representative staining). MMP3 expression was significantly higher in hormone-sensitive and HR tumors compared with PIN and normal tissue (Fig. 4*E*). Furthermore, analysis using Spearman rank correlation demonstrated that MMP3 is significantly associated with phospho-eIF4E (ρ = 0.396) and eIF4E (ρ = 0.524) in tumor tissues (Table S3). In addition, we performed staining for p-ERK and p-AKT to examine the association between upstream signaling activity and eIF4E phosphorylation. As expected, eIF4E phosphorylation correlated with p-ERK (ρ = 0.266) and p-AKT (ρ = 0.321). Strikingly, MMP3 was not significantly associated with p-ERK (ρ = 0.006) and p-AKT (ρ = 0.110), suggesting a stronger association between p-eIF4E and MMP3 than with upstream MAPK and PI3K signaling.

Discussion

We show that eIF4E phosphorylation promotes prostate tumor development and progression in mice. mRNAs that are less well translated in the absence of eIF4E phosphorylation include those that encode for proteins involved in the remodeling of the ECM, inhibition of apoptosis, and cellular growth and proliferation. The decrease in MMP3 and the chemokine CCL2 is consistent with the reduction in invasiveness observed in the KI mice prostate tumors. eIF4E phosphorylation is strongly associated with high Gleason score (>7) and HR prostate cancer in a patient cohort, which predicts poor survival (33, 34). It is well established that

eIF4E is overexpressed in many human tumors, including prostate cancer (35), and this was also shown here by using TMAs of patients with prostate cancer. However, an increase in the amount of eIF4E is not sufficient for transformation, as eIF4E must be phosphorylated by MNKs. The Oncomine database (36) documents that *MNK2* is overexpressed 1.5- to 4.4-fold in HR and metastatic prostate tumors (37–39). Moreover, MNK activity promotes proliferation in prostate cancer cells (40). This is expected to contribute to the increase in eIF4E phosphorylation seen in tumors with high Gleason scores, considering that MNK2 constitutively phosphorylates eIF4E (41).

Previous work has demonstrated that eIF4E phosphorylation is not required for translation under standard growth conditions (41). However, many studies documented a positive correlation between increased eIF4E phosphorylation and cell proliferation and enhanced translation (42, 43). Here, we identified mRNAs that are preferentially responsive to eIF4E phosphorylation for maximal translation. Future work will be needed to identify the mechanisms that render the translation of these mRNAs more sensitive to eIF4E phosphorylation. Several studies have demonstrated that p-eIF4E binds with lower affinity to the cap structure (44–46). Although this finding is counterintuitive, it was proposed that the decreased affinity could stimulate translation by releasing eIF4E from the cap, akin to the mechanism of promoter clearing during transcription initiation (47).

In a preclinical mouse model of prostate cancer, inhibition of mTOR and ERK signaling pathways using a combination therapy of rapamycin and PD0325901 impaired tumor growth (48). We demonstrated that the phosphorylation of eIF4E is regulated by these two signaling pathways; therefore, inhibition of eIF4E phosphorylation as a treatment for cancer is a very intriguing idea, considering that it does not have a conspicuous effect on normal proliferation.

Materials and Methods

IHC. IHC was performed using the Vectastain Elite ABC kit (Vector Laboratories) according to the manufacturer's instructions. Antibodies were used at the following dilutions: p-eIF4E 1:500 (Novus Biologicals), MMP3 1:250 (Abcam), CCL2 1:100 (Novus Biologicals), eIF4E 1:400 (CST), p-AKT S473 1:50
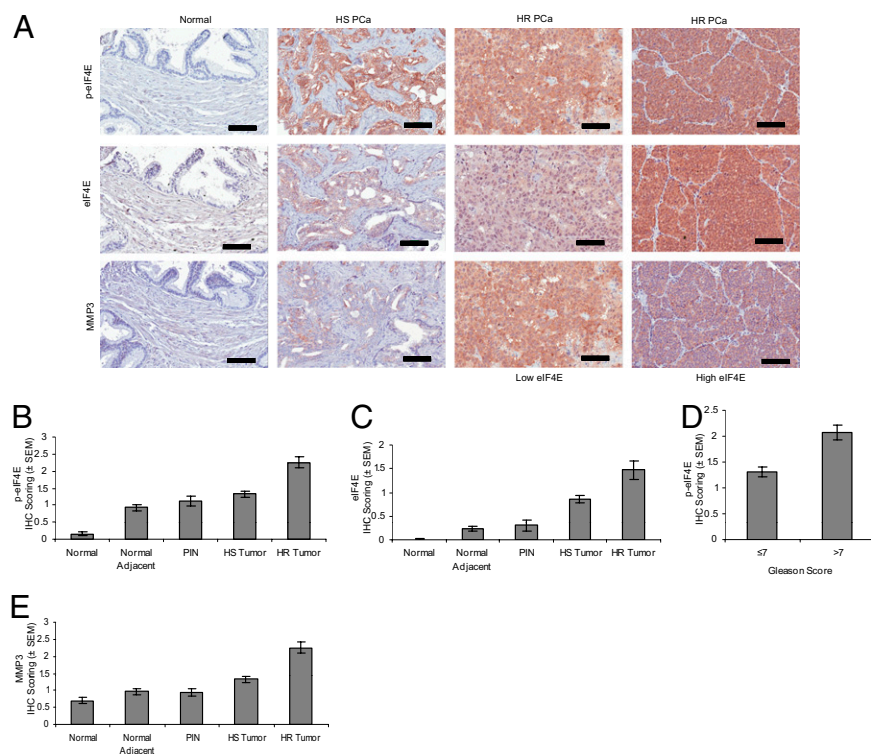
Fig. 4. p-eIF4E correlates with progression to HR PCa. eIF4E, phospho-eIF4E, and MMP3 were detected by IHC in human prostate cancer TMAs. The intensity of staining was scored from 0 to 4 for each core and data were analyzed as described in *Materials and Methods*. (*A*) Representative images of staining intensity obtained for eIF4E and p-eIF4E. (Scale bar: 100 μm.) (*B* and *C*) eIF4E and phospho-eIF4E immunoreactivity shows a gradual increase in intensity from the normal, normal adjacent, PIN, HS tumor, and HR tumor tissues. Significant statistical differences were found between the different histopathological groups ($P < 0.001$, Kruskal-Wallis test). (*D*) The mean intensity difference of phospho-eIF4E in cases with Gleason score greater than 7 compared with Gleason scores of 7 or lower is statistically significant ($P < 0.05$, Mann–Whitney *U* test). (*E*) MMP3 immunoreactivity is gradually increased in intensity from PIN to HS tumor and HR tumor tissues. Significant statistical differences exist between the different histopathological groups ($P < 0.001$, Kruskal-Wallis test).

Furic et al.

(CST), and Ki67 1:2,000 (Novocastra). SMA detection was performed with the Mouse-On-Mouse kit (Vector Laboratories) according to the manufacturer's instructions. SMA antibody (Dako) was used at 1:500.

Western Blotting. Primary antibodies were used at the following dilutions: pan-AKT 1:1,000 (CST), p-AKT S473 1:1,000 (CST), eIF4E 1:1,000 (CST), NFKBIA 1:1,000 (CST), BIRC2 1:1,000 (Novus Biologicals), p-eIF4E 1:5,000 (Novus Biologicals), MMP3 1:500 (Abcam), β-actin 1:10,000 (Sigma), VEGFC 1:250 (Abcam), RAPTOR 1:1,000 (CST), 4E-BP1 1:1,000 (CST), rpS6 1:5,000 (Santa Cruz Biotechnology), and p-rpS6[240/244] 1:1,000 (CST).

Transformation Assays. c-Myc-, E1A-, Ras^{V12}-, SV40 largeT-, CRE-, and HA-eIF4E–expressing retroviruses were generated by transfecting packaging Phoenix cells with the following plasmids: pBabe-c-Myc, pBabe-HA-eIF4E, pLpc-E1A/Ras^{V12}, pWzl-Ras^{V12}, pMSCV-CRE, and pSV40T (Myc-, E1A-, and Ras^{V12}-expressing plasmids were gifts of Scott Lowe, Cold Spring Harbor

Laboratory, NY; pSV40T was a gift of Julian Downward, London Research Institute, UK). MEFs were infected with retroviruses three times over a 48-h period and pools of infected cells were selected by two rounds of selection with puromycin for pBabe, hygromycin for pWzl, or G418 for pMSCV.

1. Mamane Y, Petroulakis E, LeBacquer O, Sonenberg N (2006) mTOR, translation initiation and cancer. *Oncogene* 25:6416–6422.
2. De Benedetti A, Graff JR (2004) eIF-4E expression and its role in malignancies and metastases. *Oncogene* 23:3189–3199.
3. Clemens MJ (2004) Targets and mechanisms for the regulation of translation in malignant transformation. *Oncogene* 23:3180–3188.
4. Schneider RJ, Sonenberg N (2007) Translational control in cancer development. *Control in Biology and Medicine*, eds Mathews MB, Sonenberg N, Hershey JWB (Cold Spring Harbor Lab Press, Cold Spring Harbor, NY), pp 401–432.
5. Lazaris-Karatzas A, Montine KS, Sonenberg N (1990) Malignant transformation by a eukaryotic initiation factor subunit that binds to mRNA 5′ cap. *Nature* 345:544–547.
6. Avdulov S, et al. (2004) Activation of translation complex eIF4F is essential for the genesis and maintenance of the malignant phenotype in human mammary epithelial cells. *Cancer Cell* 5:553–563.
7. Ruggero D, et al. (2004) The translation factor eIF-4E promotes tumor formation and cooperates with c-Myc in lymphomagenesis. *Nat Med* 10:484–486.
8. Wendel HG, et al. (2004) Survival signalling by Akt and eIF4E in oncogenesis and cancer therapy. *Nature* 428:332–337.
9. Waskiewicz AJ, Flynn A, Proud CG, Cooper JA (1997) Mitogen-activated protein kinases activate the serine/threonine kinases Mnk1 and Mnk2. *EMBO J* 16:1909–1920.
10. Fukunaga R, Hunter T (1997) MNK1, a new MAP kinase-activated protein kinase, isolated by a novel expression screening method for identifying protein kinase substrates. *EMBO J* 16:1921–1933.
11. Topisirovic I, Ruiz-Gutierrez M, Borden KL (2004) Phosphorylation of the eukaryotic translation initiation factor eIF4E contributes to its transformation and mRNA transport activities. *Cancer Res* 64:8639–8642.
12. Wendel HG, et al. (2007) Dissecting eIF4E action in tumorigenesis. *Genes Dev* 21:3232–3237.
13. Waskiewicz AJ, et al. (1999) Phosphorylation of the cap-binding protein eukaryotic translation initiation factor 4E by protein kinase Mnk1 in vivo. *Mol Cell Biol* 19:1871–1880.
14. Gingras AC, Raught B, Sonenberg N (2004) mTOR signaling to translation. *Curr Top Microbiol Immunol* 279:169–197.
15. Trotman LC, et al. (2003) Pten dose dictates cancer progression in the prostate. *PLoS Biol* 1:E59.
16. Thoreen CC, et al. (2009) An ATP-competitive mammalian target of rapamycin inhibitor reveals rapamycin-resistant functions of mTORC1. *J Biol Chem* 284:8023–8032.
17. Feldman ME, et al. (2009) Active-site inhibitors of mTOR target rapamycin-resistant outputs of mTORC1 and mTORC2. *PLoS Biol* 7:e38.
18. Pyronnet S, et al. (1999) Human eukaryotic translation initiation factor 4G (eIF4G) recruits mnk1 to phosphorylate eIF4E. *EMBO J* 18:270–279.
19. Couto SS, Raught B, Sonenberg N (2009) Simultaneous haploinsufficiency of Pten and Trp53 tumor suppressor genes accelerates tumorigenesis in a mouse model of prostate cancer. *Differentiation* 77:103–111.
20. Park JH, et al. (2002) Prostatic intraepithelial neoplasia in genetically engineered mice. *Am J Pathol* 161:727–735.
21. Price D (1963) Comparative aspects of development and structure in the prostate. *Natl Cancer Inst Monogr* 12:1–27.
22. Haffner J, et al. (2009) Peripheral zone prostate cancers: Location and intraprostatic patterns of spread at histopathology. *Prostate* 69:276–282.
23. McNeal JE, Redwine EA, Freiha FS, Stamey TA (1988) Zonal distribution of prostatic adenocarcinoma. Correlation with histologic pattern and direction of spread. *Am J Surg Pathol* 12:897–906.
24. Li X, et al. (2009) A destructive cascade mediated by CCL2 facilitates prostate cancer growth in bone. *Cancer Res* 69:1685–1692.
25. Loberg RD, et al. (2007) Targeting CCL2 with systemic delivery of neutralizing antibodies induces prostate cancer tumor regression in vivo. *Cancer Res* 67:9417–9424.
26. Van Damme J, Proost P, Lenaerts JP, Opdenakker G (1992) Structural and functional identification of two human, tumor-derived monocyte chemotactic proteins (MCP-2 and MCP-3) belonging to the chemokine family. *J Exp Med* 176:59–65.
27. Singh S, Singh UP, Grizzle WE, Lillard JW, Jr (2004) CXCL12-CXCR4 interactions modulate prostate cancer cell migration, metalloproteinase expression and invasion. *Lab Invest* 84:1666–1676.
28. Wilson TJ, Singh RK (2008) Proteases as modulators of tumor-stromal interaction: primary tumors to bone metastases. *Biochim Biophys Acta* 1785:85–95.
29. Radisky DC, et al. (2005) Rac1b and reactive oxygen species mediate MMP-3-induced EMT and genomic instability. *Nature* 436:123–127.
30. Rowlett RM, et al. (2008) MNK kinases regulate multiple TLR pathways and innate proinflammatory cytokines in macrophages. *Am J Physiol Gastrointest Liver Physiol* 294:G452–G459.
31. Le Page C, Koumakpayi IH, Alam-Fahmy M, Mes-Masson AM, Saad F (2006) Expression and localisation of Akt-1, Akt-2 and Akt-3 correlate with clinical outcome of prostate cancer patients. *Br J Cancer* 94:1906–1912.
32. Diallo JS, et al. (2007) NOXA and PUMA expression add to clinical markers in predicting biochemical recurrence of prostate cancer patients in a survival tree model. *Clin Cancer Res* 13:7044–7052.
33. Lau WK, Bergstralh EJ, Blute ML, Slezak JM, Zincke H (2002) Radical prostatectomy for pathological Gleason 8 or greater prostate cancer: Influence of concomitant pathological variables. *J Urol* 167:117–122.
34. Oefelein MG, Agarwal PK, Resnick MI (2004) Survival of patients with hormone refractory prostate cancer in the prostate specific antigen era. *J Urol* 171:1525–1528.
35. Graff JR, et al. (2009) eIF4E activation is commonly elevated in advanced human prostate cancers and significantly related to reduced patient survival. *Cancer Res* 69:3866–3873.
36. Rhodes DR, et al. (2004) ONCOMINE: A cancer microarray database and integrated data-mining platform. *Neoplasia* 6:1–6.
37. Lapointe J, et al. (2004) Gene expression profiling identifies clinically relevant subtypes of prostate cancer. *Proc Natl Acad Sci USA* 101:811–816.
38. Tomlins SA, et al. (2007) Integrative molecular concept modeling of prostate cancer progression. *Nat Genet* 39:41–51.
39. Varambally S, et al. (2005) Integrative genomic and proteomic analysis of prostate cancer reveals signatures of metastatic progression. *Cancer Cell* 8:393–406.
40. Bianchini A, et al. (2008) Phosphorylation of eIF4E by MNKs supports protein synthesis, cell cycle progression and proliferation in prostate cancer cells. *Carcinogenesis* 29:2279–2288.
41. Ueda T, Watanabe-Fukunaga R, Fukuyama H, Nagata S, Fukunaga R (2004) Mnk2 and Mnk1 are essential for constitutive and inducible phosphorylation of eukaryotic initiation factor 4E but not for cell growth or development. *Mol Cell Biol* 24:6539–6549.
42. Flynn A, Proud CG (1996) Insulin and phorbol ester stimulate initiation factor eIF-4E phosphorylation by distinct pathways in Chinese hamster ovary cells overexpressing the insulin receptor. *Eur J Biochem* 236:40–47.
43. Gingras AC, Raught B, Sonenberg N (1999) eIF4 initiation factors: effectors of mRNA recruitment to ribosomes and regulators of translation. *Annu Rev Biochem* 68:913–963.
44. Scheper GC, et al. (2002) Phosphorylation of eukaryotic initiation factor 4E markedly reduces its affinity for capped mRNA. *J Biol Chem* 277:3303–3309.
45. Slepenkov SV, Darzynkiewicz E, Rhoads RE (2006) Stopped-flow kinetic analysis of eIF4E and phosphorylated eIF4E binding to cap analogs and capped oligoribonucleotides: Evidence for a one-step binding mechanism. *J Biol Chem* 281:14927–14938.
46. Zuberek J, et al. (2003) Phosphorylation of eIF4E attenuates its interaction with mRNA 5′ cap analogs by electrostatic repulsion: Intein-mediated protein ligation strategy to obtain phosphorylated protein. *RNA* 9:52–61.
47. Scheper GC, Proud CG (2002) Does phosphorylation of the cap-binding protein eIF4E play a role in translation initiation? *Eur J Biochem* 269:5350–5359.
48. Kinkade CW, et al. (2008) Targeting AKT/mTOR and ERK MAPK signaling inhibits hormone-refractory prostate cancer in a preclinical mouse model. *J Clin Invest* 118:3051–3064.
49. Le Bacquer O, et al. (2007) Elevated sensitivity to diet-induced obesity and insulin resistance in mice lacking 4E-BP1 and 4E-BP2. *J Clin Invest* 117:387–396.
50. Frederickson RM, Montine KS, Sonenberg N (1991) Phosphorylation of eukaryotic translation initiation factor 4E is increased in Src-transformed cell lines. *Mol Cell Biol* 11:2896–2900.
51. Miller E (2004) Apoptosis measurement by annexin v staining. *Methods Mol Med* 88:191–202.

Supporting Information

Furic et al. 10.1073/pnas.1005320107

SI Materials and Methods

Cloning of the eIF4E^{S209A} Targeting Vector. The KI DNA construct was built using amplified fragments of genomic DNA. The construct contained the serine 209 to alanine mutation in exon 8 and a Neo-TK selection cassette flanked by Frt sites within intron 7. The backbone vector, plox/frt, was previously described (1). The left flank was PCR amplified with the primers 5′-CCATTGTG-GAATGCCCTAGGCC-3′ and 5′-CGTTATAGGCGCGCCAT-GGGCTCACAGCAATTGC-3′ and then digested and ligated into the AvrII and AscI sites of the backbone vector. The right flank, which contains the point mutation, was amplified in three fragments. The first fragment (A) was amplified with primer pair 5′-GCCGCCGGTTTAAACTGATCGTGATTTGCTTGTTAC-3′ and 5′-CCTATTTTTAGTGGTGGCGCCGCTCTTTGTA-GC-3′, digested with PmeI and NarI. The second fragment (B) was amplified with the primer pair 5′-GCTACAAAGAGCGG-CGCCACCACTAAAAATAGG-3′ and 5′-CCACAATTATGT-TTAGGGATC-3′ and then digested with NarI and HindIII. Fragments A and B were inserted into the PmeI/HindIII sites of the backbone vector by triple ligation. The third fragment (C) was amplified with the primer pair 5′-GCTCCACTCCATGCAG-GAGCGG-3′ and 5′-CGCAGAGGTCGACTTGCCCCATAA-TACTCCAC-3′, digested with HindIII and SalI and ligated into the HindIII/SalI sites of the vector already containing fragments A and B. The entire right flank was digested with PmeI and SalI and ligated into PmeI/SalI sites of the left flank containing construct to generate p-eIF4E-KI S209A.

ES Cell Selection. p-eIF4E-KI S209A plasmid DNA was linearized with SalI and electroporated in 129Sv/J ES cells and selection of G418 resistant transformants was done as previously described (2). A total of 480 G418 resistant colonies were tested for recombination by Southern blotting.

Polysome Microarray Analysis. WT and KI MEFs (5×10^6 cells) were grown in DMEM supplemented with 10% FBS. Polysomal and total cytoplasmic RNA was isolated as described (3). Fractions containing mRNAs bound to more than three ribosomes were pooled and designated heavy polysomal RNA. RNA isolation was performed in two independent experiments from one pair of KI and WT MEFs. RNA quality was assessed using the Bioanalyzer Nano-Chip (Agilent), and all RNA samples were of good quality (integrity number, > 9.6). RNA (250 ng) was labeled using the one-cycle Illumina protocol and the resulting cRNA was hybridized with the "MouseRef-8_V2" BeadChip (Illumina). Data analysis was performed using the statistical environment R and the package lumi (4). Data were transformed using Variance Stabilizing Transformation and normalized using Robust Spline Normalization. Technical quality was validated and biological quality was assessed using principal components analysis, which showed good separation of the WT and the KI samples, for both the heavy polysome RNA data and the heavy polysome RNA data corrected for cytosolic RNA levels, in the first component. Correction for cytosolic RNA was performed by subtracting the log2 mean cytosolic RNA levels from the corresponding polysome RNA levels. Identification of differentially expressed genes was done using Significance Analysis of Microarrays algorithm (5). Genes that were significant (q < 15) before and after correction for the cytosolic RNA level were collected. Microarray data were deposited in the Gene Expression Omnibus database (accession no. GSE17451).

Immunoreactivity Quantification and Statistical Analysis of Human Prostate Tissue. The immunoreactivity scoring was performed by an experimenter blinded to the grade of the lesions. Scoring procedure was done as follows: each core was scored according to the staining intensity (value of 0 for absence, 1 for weak, 2 for moderate, 3 for strong staining, and 4 for very strong staining). The nonparametric Kruskal-Wallis test was used to evaluate the differences between the intensity means of the normal, normal adjacent, PIN, HS tumor, and HR tumor tissues. The mean intensity of Gleason scores (≤ 7 and >7) was also compared by Mann–Whitney U test. The nonparametric Spearman rho correlation test was used to conduct correlation analysis. All statistical tests were performed using SPSS software, version 12 (SPSS).

Statistical Analysis of Mouse Prostate Tissue. Prostate tumor sections were stained with H&E and analyzed by two histopathologists blinded to the genotype of the mice. Lesions were graded from PIN I to PIN IV and invasive. A scoring procedure was done as follows: lesions were graded from 1 (PIN I) to 5 (invasive) and the weighted average was calculated for each section by taking into account the percentage of each lesion type on the section. The global score of each mouse was calculated by averaging the score of every slides corresponding to a single mouse. The nonparametric Mann–Whitney U test was used to evaluate the differences between the WT and KI cohorts.

Cell Cycle Analysis. Cells were lysed with NPE NIM-DAPI reagent (Beckman Coulter) and analyzed by using a Cell Lab Quanta SC (Beckman Coulter) flow cytometer.

Isolation of MEFs. MEFs were isolated from 14.5-d pregnant females as previously described (6). Animal protocols were approved by the McGill University Animal Care Committee and in compliance with McGill University guidelines.

Orthophosphate Labeling. eIF4E was immunoprecipitated from $H_3{}^{32}PO_4$ metabolically labeled MEFs as previously described (7).

Mouse Tissue Processing. Mouse urogenital system was isolated en bloc and fixed for 24 h in 10% buffered formalin. Alternatively, one half of the urogenital system was dissected to isolate the ventral, anterior, and dorsolateral lobes of the prostate. Tissues were paraffin-embedded, and 5-μm sections were used for H&E staining and IHC.

shRNA-Mediated Knockdown of RAPTOR. shRNA vectors (RAPTOR 1857 and Scrambled 1864; 7 μg; Addgene) were cotransfected into HEK293T cells in 100-mm dishes with lentivirus packaging plasmids PLP1, PLP2, and PLP-VSVG (7 μg of each; Invitrogen) using Lipofectamine 2000 (Invitrogen). Supernatant was collected 48 h and 72 h after transfection, passed through a 0.45-μm nitrocellulose filter, and applied on target cells with Polybrene (5 μg/mL). Cells were reinfected the next day and selected with puromycin for 48 h (1 μg/mL; Sigma).

Apoptosis Induction. Subconfluent layers of MEFs were treated with ionomycin for 24 h. Annexin V and PI staining was performed using Annexin-V-FLUOS staining kit (Roche Diagnostics) according to the manufacturer's instructions. The percentage of apoptotic and necrotic cells was determined as described (8).

Patient Cohort and TMA Construction. The TMA used for IHC was previously described (9, 10). Briefly, the specimen cohort, consisting

of 601 one-mm-wide cores of prostate tissue, was used for IHC studies. The TMA was constructed with cores representing 43 pa-

tients with normal prostate tissues, 62 patients presenting primary PCa tissues, and 30 patients with HR PCa, for a total of 135 patients.

1. Brown EJ, Baltimore D (2003) Essential and dispensable roles of ATR in cell cycle arrest and genome maintenance. *Genes Dev* 17:615–628.
2. Ramírez-Solis R, Davis AC, Bradley A (1993) Gene targeting in embryonic stem cells. *Methods Enzymol* 225:855–878.
3. Larsson O, et al. (2007) Eukaryotic translation initiation factor 4E induced progression of primary human mammary epithelial cells along the cancer pathway is associated with targeted translational deregulation of oncogenic drivers and inhibitors. *Cancer Res* 67:6814–6824.
4. Du P, Kibbe WA, Lin SM (2008) lumi: A pipeline for processing Illumina microarray. *Bioinformatics* 24:1547–1548.
5. Tusher VG, Tibshirani R, Chu G (2001) Significance analysis of microarrays applied to the ionizing radiation response. *Proc Natl Acad Sci USA* 98:5116–5121.
6. Le Bacquer O, et al. (2007) Elevated sensitivity to diet-induced obesity and insulin resistance in mice lacking 4E-BP1 and 4E-BP2. *J Clin Invest* 117:387–396.
7. Frederickson RM, Montine KS, Sonenberg N (1991) Phosphorylation of eukaryotic translation initiation factor 4E is increased in Src-transformed cell lines. *Mol Cell Biol* 11:2896–2900.
8. Miller E (2004) Apoptosis measurement by annexin v staining. *Methods Mol Med* 88:191–202.
9. Le Page C, Koumakpayi IH, Alam-Fahmy M, Mes-Masson AM, Saad F (2006) Expression and localisation of Akt-1, Akt-2 and Akt-3 correlate with clinical outcome of prostate cancer patients. *Br J Cancer* 94:1906–1912.
10. Diallo JS, et al. (2007) NOXA and PUMA expression add to clinical markers in predicting biochemical recurrence of prostate cancer patients in a survival tree model. *Clin Cancer Res* 13:7044–7052.
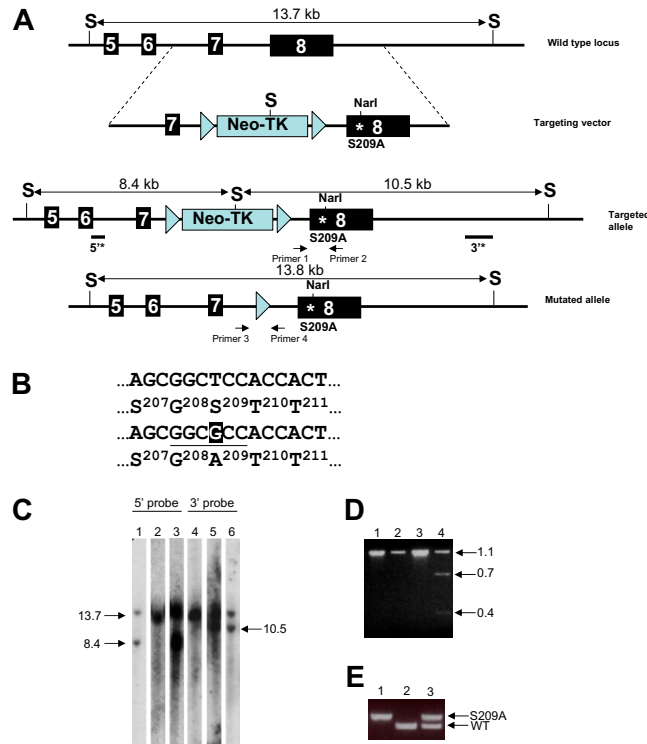
Fig. S1. Generation of a KI mouse expressing non phosphorylatable eIF4E. (*A*) A targeting vector containing the genomic DNA encompassing exons 7 and 8 of mouse eIF4E was used to introduce the mutated serine 209 into the eIF4E locus (S, SacI restriction site). (*B*) The introduction of a single nucleotide mutation in S209 codon generated a new NarI restriction site (underlined) into exon 8. (*C*) Southern blotting was performed using 5′ and 3′ specific probes on SacI-digested DNA isolated from ES cells or mouse tails to test for proper insertion/recombination of the targeting vector in the eIF4E locus on chromosome 3. Lanes 1 and 6, ES cells heterozygous for the KI mutation; lanes 2 and 4, WT mice; lanes 3 and 5, KI heterozygote mice. For a WT allele, 5′ and 3′ probes hybridize to a 13.7-kb fragment. For a KI allele, 5′ probe hybridizes to a 8.4-kb fragment and 3′ probe hybridizes to a 10.5-kb fragment. (*D*) Digestion of a PCR product amplified from oligonucleotides flanking the S209 codon shows that only the recombined allele containing the S209A mutation is cut by NarI. PCR genotyping with primer 1 and 2 produced a 1.1-kb product [lane 1 (WT mouse) and lane 3 (KI heterozygote mouse)]. Digestion of the 1.1-kb PCR product from the KI allele with NarI yielded 0.7- and 0.4-kb bands (compare lane 4 vs. lane 2). (*E*) Lanes 1 through 3 show PCR products obtained using primers 3 and 4 flanking the Frt sites, confirming the removal of the TK-Neo cassette. Lane 1, homozygous KI mouse; lane 2, WT mouse; lane 3, heterozygote KI mouse.

Fig. S2. Apoptosis and cell cycle analysis of immortalized and transformed WT and KI MEFs. (*A*) Detection of apoptotic cells by Annexin V/PI costaining. MEFs of the indicated genotype (2×10^5 cells) were grown for 24 h, collected, and analyzed by flow cytometry to detect Annexin V and PI staining. (*B*) Cell cycle analysis. MEFs of the indicated genotype (2×10^5 cells) were grown for 24 h, collected, and analyzed by flow cytometry to detect DAPI staining. (*C*) Percentage of cells in each phase of the cell cycle.

C

Cell line	Sub G0	G0/G1	S phase	G2/M
KI/PTEN^F/F SV40 Cre	3.92%	46.11%	21.17%	25.35%
WT/PTEN^F/F SV40 Cre	1.68%	46.35%	22.79%	24.76%
KI p53 null	1.10%	41.72%	14.56%	38.94%
WT p53 null	2.09%	43.12%	15.89%	35.41%
KI c-MYC+RAS^V12	1.38%	56.09%	22.17%	18.35%
WT c-MYC+RAS^V12	1.04%	57.05%	19.79%	18.80%

Fig. S3. Representative microphotographs of the seminal vesicle (SV) and of the ventral (VP), anterior (AP), and DLP lobes from the prostate of WT and KI mice. (Scale bar: 100 μm.)

Fig. S4. Representative microphotographs of the lesions observed and their grading from PIN I to PIN IV and invasive.

Fig. S5. LNCaP and LNAI prostate cancer cells were serum starved for 16 h. Cells were refed with 10% serum 1 h after the addition of the indicated inhibitors. Two hours after serum addition, cells were lysed and proteins were resolved by SDS/PAGE followed by Western blot analysis to detect the indicated proteins.

Table S1. Age of mice at the time they were euthanized

Type	5 mo	6 mo	7 mo	Median age, wk
WT/cPten^{F/F}	5	2	0	20
KI/cPten^{F/F}	2	3	2	25

Table S2. List of mRNAs more actively translated in WT compared with KI MEFs

Gene symbol	Fold change	Description
8430410K20Rik	5.09	RIKEN cDNA 8430410K20 gene
Enpp2	4.41	Ectonucleotide pyrophosphatase/phosphodiesterase 2
Dcn	4.05	Decorin
Birc2	3.54	Baculoviral IAP repeat-containing 2
Casp4	3.51	Caspase 4, apoptosis-related cysteine peptidase
Ccl7	3.36	Chemokine (C-C motif) ligand 7
Upp1	2.80	Uridine phosphorylase 1
C3	2.72	Complement component 3
Cbr3	2.51	Carbonyl reductase 3
Mmp3	2.46	Matrix metallopeptidase 3
Ccl2	2.42	Chemokine (C-C motif) ligand 2
Slco4a1	2.39	Solute carrier organic anion transporter family, member 4a1
Cd82	2.29	CD82 antigen
Adh7	2.16	Alcohol dehydrogenase 7 (class IV), mu or sigma polypeptide
Lxn	2.15	Latexin
Cyp1b1	2.12	Cytochrome P450, family 1, subfamily b, polypeptide 1
Serpina3g	2.07	Serine (or cysteine) peptidase inhibitor, clade A, member 3G
Sfrs3	2.03	Splicing factor, arginine/serine-rich 3 (SRp20)
Thbs2	2.02	Thrombospondin 2
Nfkbia	1.92	Nuclear factor of κ-light polypeptide gene enhancer in B-cells inhibitor, alpha
Prl2c4	1.92	Prolactin family 2, subfamily c, member 4
Zfp36l1	1.79	Zinc finger protein 36, C3H type-like 1
Bxdc1	1.74	Brix domain containing 1
Vegfc	1.73	Vascular endothelial growth factor C
Sssca1	1.71	Sjogren syndrome/scleroderma autoantigen 1 homologue (human)
Plk2	1.70	Polo-like kinase 2 (Drosophila)
Prl2c3	1.67	Prolactin family 2, subfamily c, member 3
Arhgef3	1.66	Rho guanine nucleotide exchange factor (GEF) 3
Ccl9	1.61	Chemokine (C-C motif) ligand 9
Dcun1d5	1.58	DCN1, defective in cullin neddylation 1, domain containing 5 (Saccharomyces cerevisiae)
Pdgfra	1.57	Platelet derived growth factor receptor, alpha polypeptide
Slc24a3	1.56	Solute carrier family 24 (sodium/potassium/calcium exchanger), member 3
Mtvr2	1.55	Mammary tumor virus receptor 2
Mmp9	1.53	Matrix metallopeptidase 9
Rbmx	1.51	RNA binding motif protein, X chromosome

Table S3. Correlation analysis among pERK, pAKT, MMP3, peIF4E, and eIF4E in prostate cancer tumor tissues

Comparison	pERK	pAKT	MMP3	peIF4E	eIF4E
pERK					
Correlation coefficient	1	0.258*	0.006	0.266*	0.244
Significance	–	0.046	0.966	0.038	0.058
pAKT					
Correlation coefficient	0.258*	1	0.11	0.321*	0.395**
Significance	0.046	–	0.399	0.011	0.002
MMP3					
Correlation coefficient	0.006	0.11	1	0.396**	0.524**
Significance	0.966	0.399	–	0.001	<0.001
peIF4E					
Correlation coefficient	0.266*	0.321*	0.396**	1	0.550**
Significance	0.038	0.011	0.001	–	0
eIF4E					
Correlation coefficient	0.244	0.395**	0.524**	0.550**	1
Significance	0.058	0.002	<0.001	<0.001	–

Correlation is significant at the *0.05 level or **0.01 level (two-tailed P value). Correlation coefficient is the Spearman ρ.

8. Supporting Data

Fig. 1
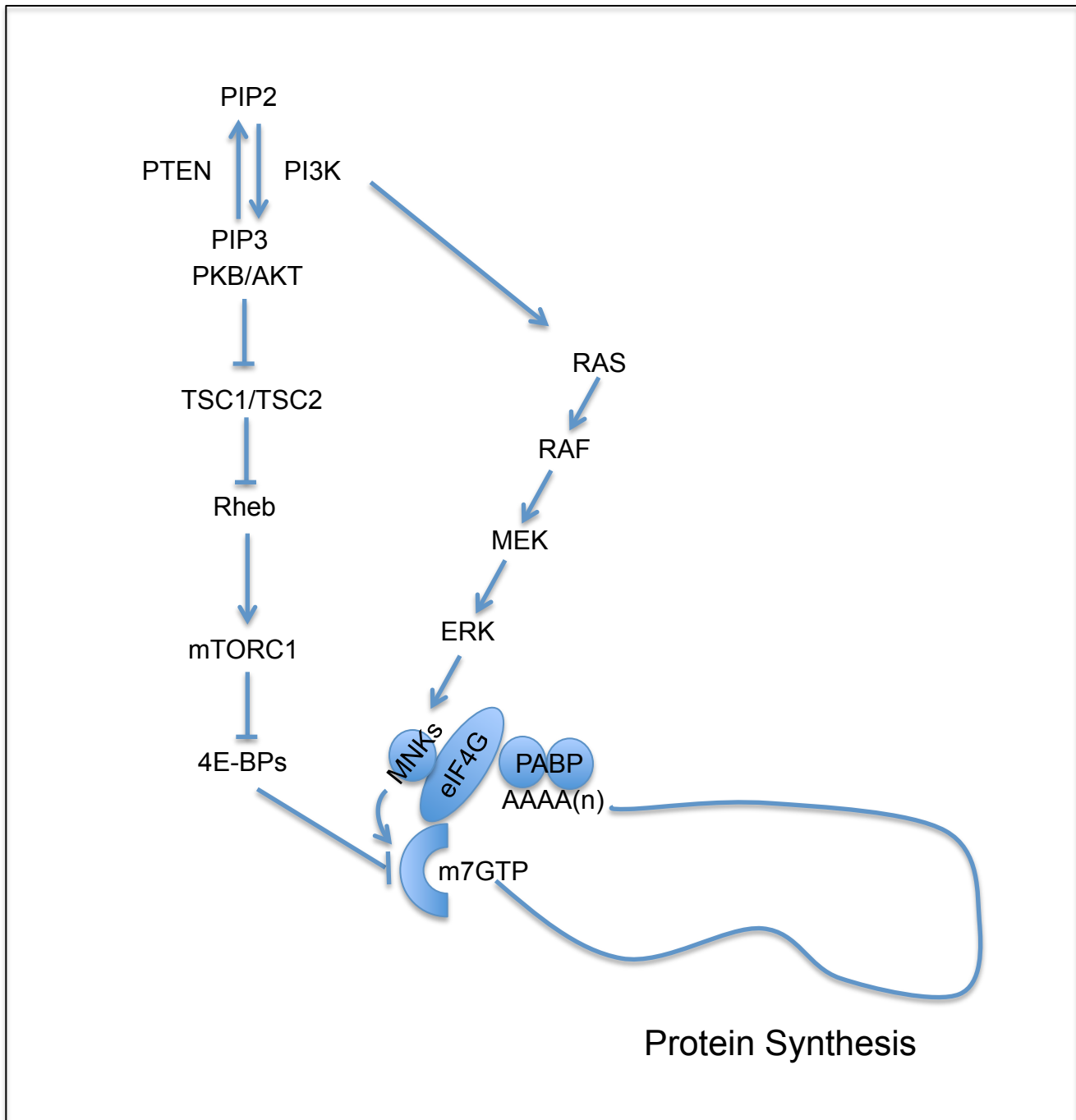
Fig. 1. Schematic representation of signaling pathways upstream of eIF4E. PI3K/AKT/mTORC1 signaling pathway regulates phosphorylation of 4E-BPs and their binding to eIF4E. RAS/RAF/MEK/ERK/MNKs pathway phosphorylate Ser^{209} on eIF4E to regulate eIF4E cap-binding and prostate cancer development.
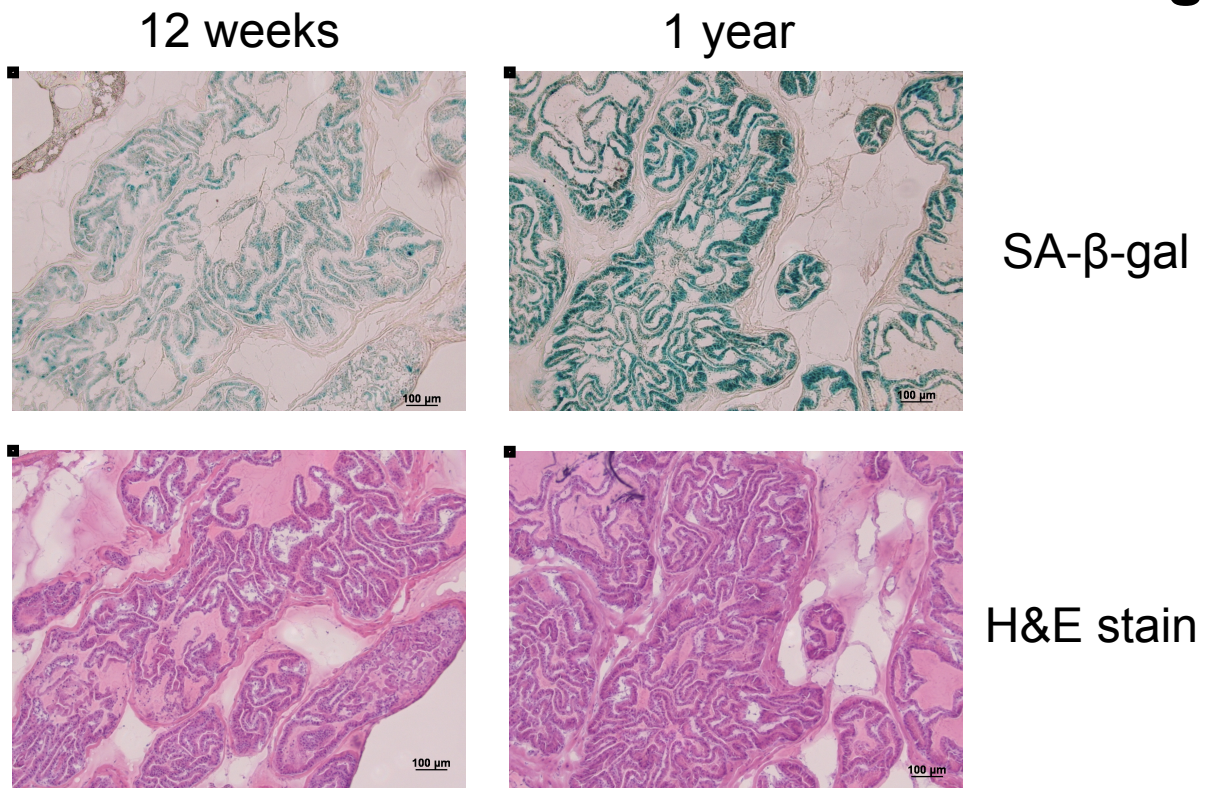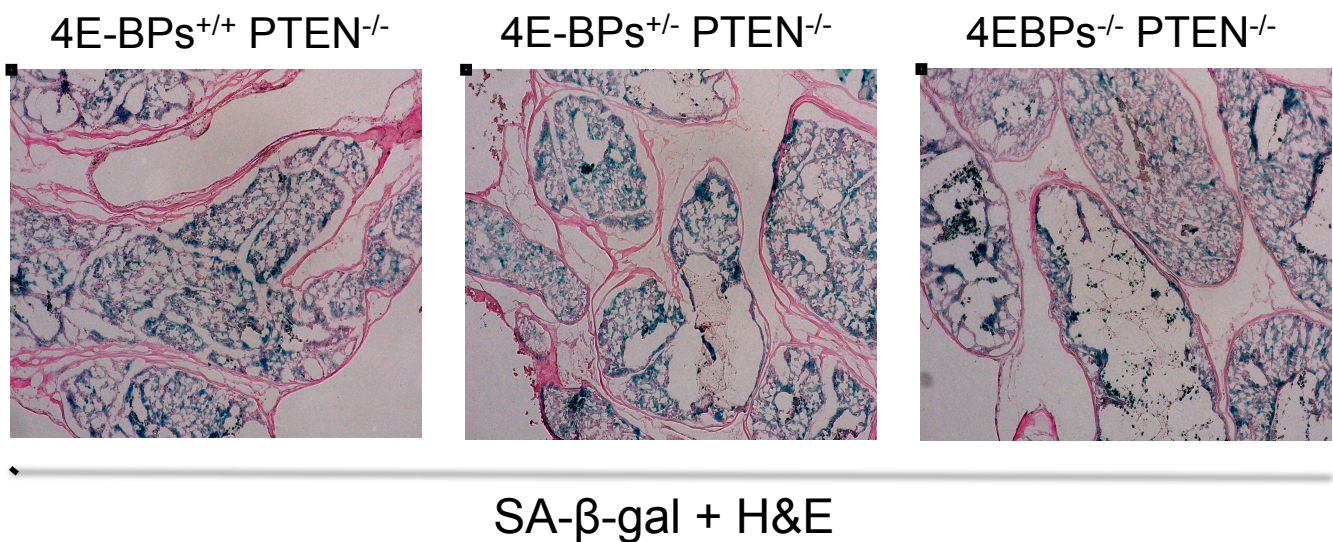
Fig. 2. SA-β-gal and H&E staining of mouse prostate sections. (A) Prostate sections of 12-week old and 1-year old wildtype mice were stained for SA-β-gal and H&E. **(B)** SA-β-gal and H&E staining of prostate sections of wildtype 4E-BP1/4E-BP2, heterozygous 4E-BP1/4E-BP2 and 4E-BP1/4E-BP2 null mice (in a PTEN-null background).

Fig. 3

A

Soft agar assay (PC3 cells)

Number of colonies vs. DMSO, RAPA, PP242, CPD3, RAPA +CPD3, PP242 +CPD3

B

(P) S6

β-actin

DMSO, RAPA, PP242, CPD3, RAPA + CPD3, PP242 + CPD3
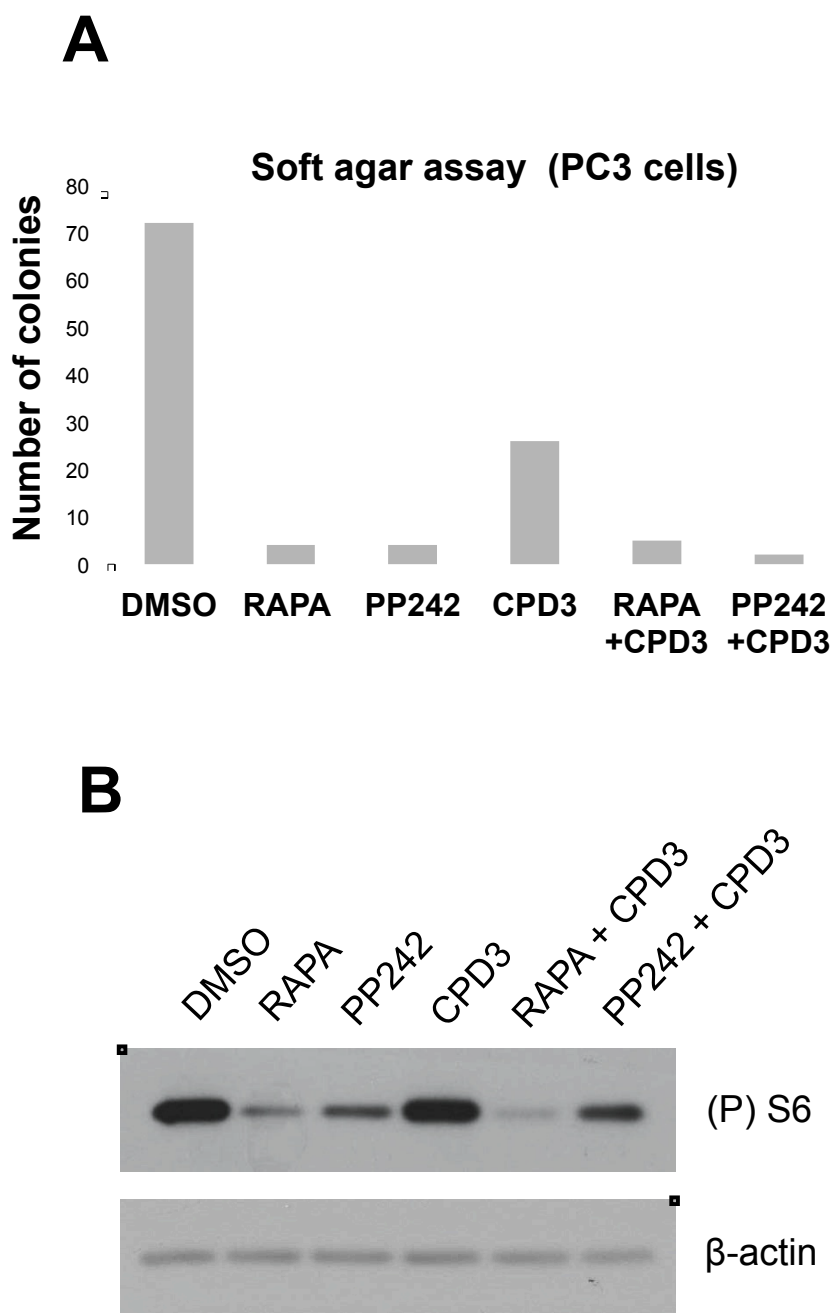
Fig. 3. Anchorage-independent growth of human prostate cancer (PC-3) cell line treated with mTOR and Mnk inhibitors. (A) PC-3 cells were incubated with 10 nM rapamycin, 2.5 µM PP242 and/or 10 µM compound 3. Anchorage-independent growth using the soft-colony formation assay. **(B)** Samples of lysates were analysed for mTORC1 activation by Western blot with the antisera indicated.